

Mechanism-based design of precursors for focused electron beam-induced deposition

Will G. Carden, and **Hang Lu**, Department of Chemistry, University of Florida, Gainesville, Florida 32611-7200, USA
Julie A. Spencer, Department of Chemistry, Johns Hopkins University, Baltimore, Maryland 21218-2685, USA; Department of Chemistry, United States Naval Academy, Annapolis, Maryland 21402, USA
D. Howard Fairbrother, Department of Chemistry, Johns Hopkins University, Baltimore, Maryland 21218-2685, USA
Lisa McElwee-White, Department of Chemistry, University of Florida, Gainesville, Florida 32611-7200, USA

Address all correspondence to Lisa McElwee-White at lmwhite@chem.ufl.edu

(Received 22 February 2018; accepted 10 April 2018)

Abstract

Focused electron beam-induced deposition (FEBID) is capable of producing metal-containing nanostructures with lateral resolution on the sub-nanometer scale. Practical application of this nanofabrication technique has been hindered by ligand-derived contamination from precursors developed for thermal deposition methods. Mechanistic insight into FEBID through surface science studies and gas-phase electron–molecule interactions has begun to enable the design of custom FEBID precursors. These studies have shown that precursors designed to decompose under electron irradiation can produce high-purity FEBID deposits. Herein, we highlight the progress in FEBID precursor development with several examples that incorporate this mechanism-based design approach.

Introduction

Focused electron beam-induced deposition (FEBID) is a promising nanofabrication technique that can create metal-containing nanostructures by using electrons to induce local decomposition of organometallic precursors adsorbed onto solid substrates in a vacuum environment.^[1] The precursor molecules are physisorbed onto the surface under (local) steady-state conditions in dynamic equilibrium with the gas feed and serve as the reactant for the intended deposit. Deposition is initiated when secondary electrons created by the interaction of the primary electron beam with the substrate stimulate the decomposition of molecularly adsorbed precursor molecules into non-volatile fragments.^[2–5] A representation of the FEBID process is depicted in [Fig. 1](#).

FEBID combines the advantages of direct-write lithographic processes (e.g., high spatial resolution, site specificity, maskless, resistless) with the flexibility to deposit materials on non-planar surfaces. The lateral dimensions of the deposits are controlled by rastering the electron beam, while the vertical dimensions are controlled by varying the dwell time at a specific location.^[2–5] Consequently, FEBID has the capability to fabricate deposits where the size, shape, and interparticle distance can all be accurately and independently controlled across a range of length scales due to the relative ease with which electrons can be focused and translated. As such, a virtually unlimited range of spatially and geometrically well-defined three-dimensional (3D) metal-containing nanostructures with potential applications in a wide array of nanotechnologies can

be created by FEBID. Consequently, FEBID is increasingly being used to fabricate and prototype freestanding, single-nanometer scaled nanostructures ([Fig. 2](#)).^[6–10] Indeed, nanostructures created by FEBID have already garnered broad usage, including a commercial system for repairing extreme ultraviolet lithography masks,^[11–14] customized tips for local probe microscopes,^[15,16] and the fabrication and modification of nanophotonic and nanoplasmonic devices.^[17–19] The potential of FEBID to impact various nanotechnologies has been further enhanced by the development of multi-beam technologies that could transform FEBID into a parallel processing technique for creating nanostructured arrays and devices for larger scale technologic applications.^[20]

Ultra-high vacuum studies on commercially available chemical vapor deposition precursors

Mechanism-based precursor design^[23,24] relies on the mechanistic information about precursor decomposition under the reaction conditions of the particular deposition technique. For FEBID, the critical information involves electron–molecule interactions. To gain insight into mechanistic details of the FEBID process, an ultra-high vacuum (UHV) surface science approach^[25,26] has been used ([Fig. 3](#)), in which vapor phase precursor molecules are adsorbed onto a cold substrate to generate a 1–2 monolayer (ML) film. Use of a cold substrate (<200 K) minimizes the likelihood of thermal reactions or precursor decomposition upon adsorption as well as thermal effects

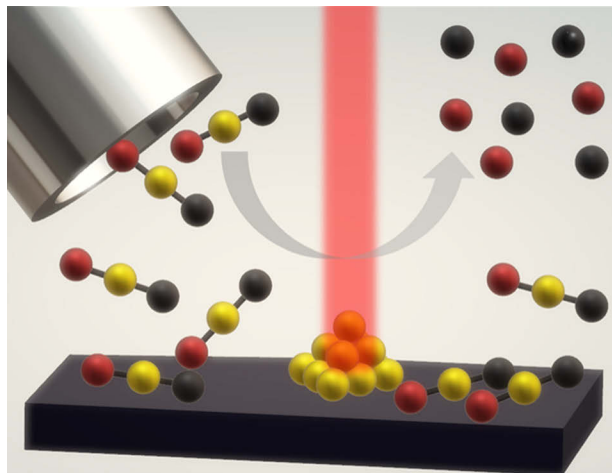


Figure 1. An illustration of FEBID of metallic gold from $X\text{-Au-L}$ precursors. $X\text{-Au-L}$ precursors are introduced through the gas injection system (GIS) and are physisorbed onto the substrate surface. Electron beam irradiation stimulates precursor decomposition producing volatile X and L species that desorb from the surface and a non-volatile Au deposit. The gold spheres represent gold atoms, the burgundy spheres represent X -type ligands (e.g., Cl, Br, I), and the black spheres represent L -type ligands (e.g., PR_3 , CO, CNR, where R = alkyl or aryl).

such as diffusion. Under these conditions, experimental results can be reasonably attributed to electron-stimulated reactions. By using a broad beam electron source (flood gun) to irradiate adsorbed precursor films, X-ray photoelectron spectroscopy (XPS) can be used to monitor surface reactions, while mass spectrometry (MS) detects species desorbed by the action of the electron beam. The energy of the electrons generated by the flood gun (500 eV) is sufficient to generate the low-energy secondary electrons (energies $< \sim 100$ eV) that are widely believed to be responsible for the elementary reaction steps that accompany FEBID.^[27–29]

The UHV surface science approach^[25,26] provides details of the reactions that occur during electron-induced precursor

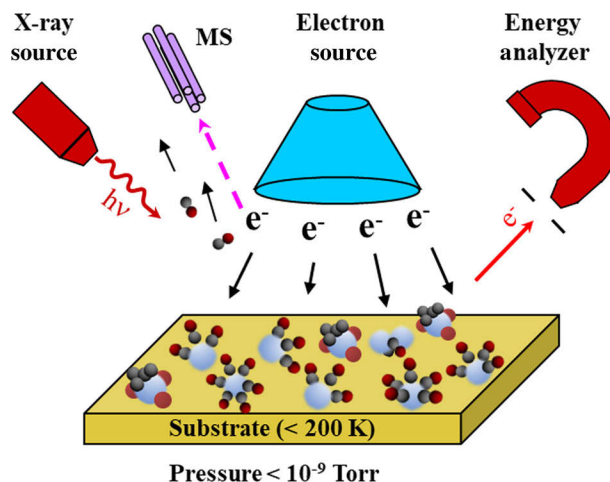


Figure 3. Applying a UHV surface science approach to FEBID. A 1–2 monolayer film of precursor molecules is adsorbed at low temperatures (< 200 K) and exposed to a broad beam source of incident electrons; changes in the film composition and bonding are probed with XPS while mass spectrometry identifies gas-phase species that desorb as a result of electron irradiation.

decomposition that are not available in a typical FEBID apparatus. Generally, FEBID is performed in a modified scanning electron microscope, in a pressure range of 10^{-5} to 10^{-6} Torr, with a constant partial pressure of precursor during deposition, at ambient temperature.^[1–5] Since surface science studies are conducted in UHV (base pressure $< 5 \times 10^{-9}$ Torr), the presence of background gases that are typically present in electron microscopes is negligible, allowing MS to detect and discern species generated as a result of electron irradiation in the absence of overwhelming signals from background gases. In addition, the precursor coverage is fixed by the initial dose, as the precursor supply is not refreshed after the initial adsorption (physisorption) of precursor molecules. This enables the use of XPS to monitor changes in the coverage and bonding

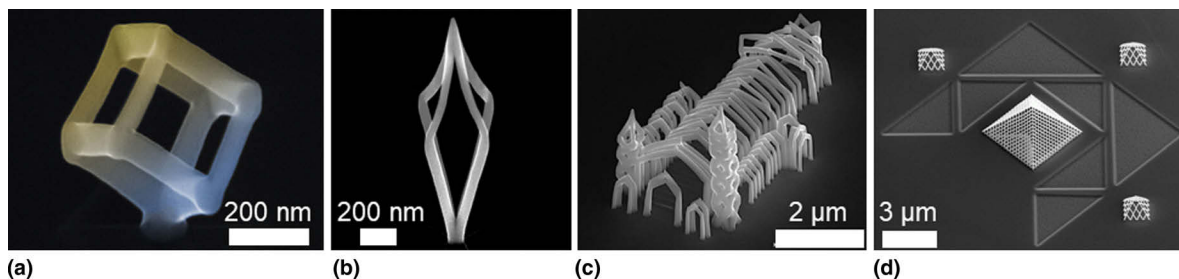


Figure 2. Representative examples of structures fabricated by FEBID. (a) Three-dimensional cube frame. Reprinted (adapted) with permission from Ref. [21]. Copyright 2016 American Chemical Society. (b) Tetragonal bipyramidal Au plasmonic structure. Reprinted (adapted) with permission from Ref. [22]. Copyright 2017 American Chemical Society. (c) Herz-Jesu-Kirche (Graz, Austria) replica made of Pt and C. Reprinted (adapted) with permission from Robert Winkler, 2015 Electron, Ion, and Photon Beam Technology and Nanofabrication (EIPBN) Conference Micrograph Contest Winner. (d) The Louvre (Paris, France) replica. Glass pyramids are made of Pt and C. Reprinted (adapted) with permission from Ref. [22]. Copyright 2017 American Chemical Society and Robert Winkler, 2016 Micro Nano Engineering (MNE) Conference Micro-Nano Graph Contest.

environments of the various elements contained within the organometallic precursor, information that can be used to determine the sequence of the reaction steps that occur as a result of electron irradiation.

To determine how FEBID precursors react under the influence of electron irradiation, UHV surface science studies initially focused on the evaluation of several widely used FEBID precursors, typically developed and used primarily for chemical vapor deposition (CVD). These CVD precursors are designed to produce pure or nearly pure metallic films in a process governed by thermal chemistry at elevated temperatures in the presence of a co-reductant or oxidant. However, the FEBID process relies on precursor–electron interactions, typically at ambient temperatures. Due to differences in these processes, precursors that produce pure metallic films in CVD often produce FEBID nanostructures with poor metal content.^[30]

Monodentate ligands: homoleptic carbonyl complexes

Many popular FEBID precursors contain exclusively monodentate ligands, where the metal center is coordinated by one donor atom of the ligand. Perhaps the most prevalent monodentate ligand encountered in FEBID precursors is the carbonyl (CO) group,^[3] found in the precursors such as $\text{Fe}(\text{CO})_5$,^[31] $\text{Co}_2(\text{CO})_8$,^[32] $\text{Mo}(\text{CO})_6$,^[33] and $\text{W}(\text{CO})_6$.^[34] Tungsten hexacarbonyl [$\text{W}(\text{CO})_6$] is a commonly used FEBID precursor that produces nanostructures comprised of oxidized tungsten atoms encased in a carbonaceous matrix.^[34–37] UHV surface science studies found that the elementary reaction steps that

lead to the formation of these deposits occur in a two-step process.^[38] Experimentally, this is shown in Fig. 4 where the evolution in the W(4f), C(1s), and O(1s) regions of adsorbed $\text{W}(\text{CO})_6$ films exposed to varying degrees of electron irradiation is plotted. Prior to electron irradiation (Fig. 4 bottom spectrum), the W(4f), C(1s), and O(1s) regions are indicative of molecularly adsorbed $\text{W}(\text{CO})_6$. After a short electron exposure, there is a little change in the W(4f) region, while the area of both the C(1s) and O(1s) regions has decreased. By following the change in integrated area within the C(1s) and O(1s) regions as a function of electron irradiation, it can be determined that two to three CO ligands per $\text{W}(\text{CO})_6$ molecule are lost from the film during this initial stage of the reaction.^[38] The loss of CO from the precursor is supported by the evolution of gas-phase CO during electron beam irradiation as shown by the MS data [Fig. 5(a)].^[38] As a result of this precursor decomposition step, partially decarbonylated surface-bound intermediates are produced [e.g., $\text{W}(\text{CO})_{4(\text{ads})}$]. Electron irradiation of these intermediates, however, does not cause further ligand desorption, but rather ligand decomposition. Thus, Fig. 4 shows that for larger electron doses, the CO contribution in both the C(1s) and O(1s) regions has largely disappeared to be replaced by spectral signatures indicative of graphitic carbon and oxidized tungsten atoms, consistent with the chemical characteristics of FEBID deposits created from $\text{W}(\text{CO})_6$.^[34–38]

Monodentate ligands: homoleptic phosphine complexes

Another example of an FEBID precursor bearing solely monodentate ligands is the tetrahedral Pt(0) trifluorophosphine

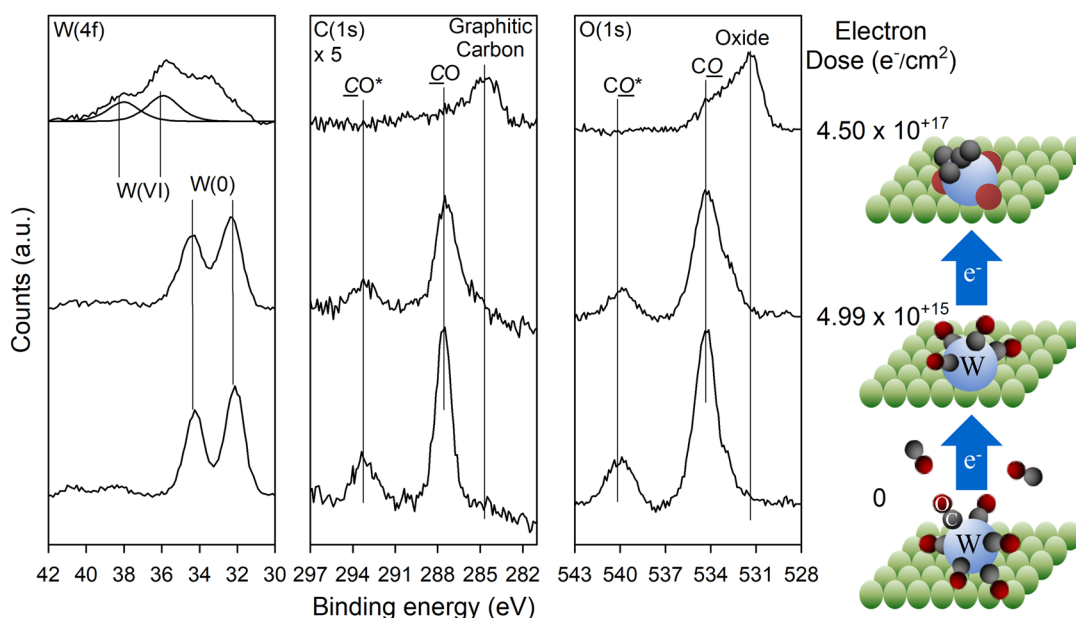


Figure 4. X-ray photoelectron spectroscopy regions for the W(4f), C(1s), and O(1s) regions as a function of electron dose (left). Corresponding state of the $\text{W}(\text{CO})_6$ adsorbate at different stages of electron irradiation (right).

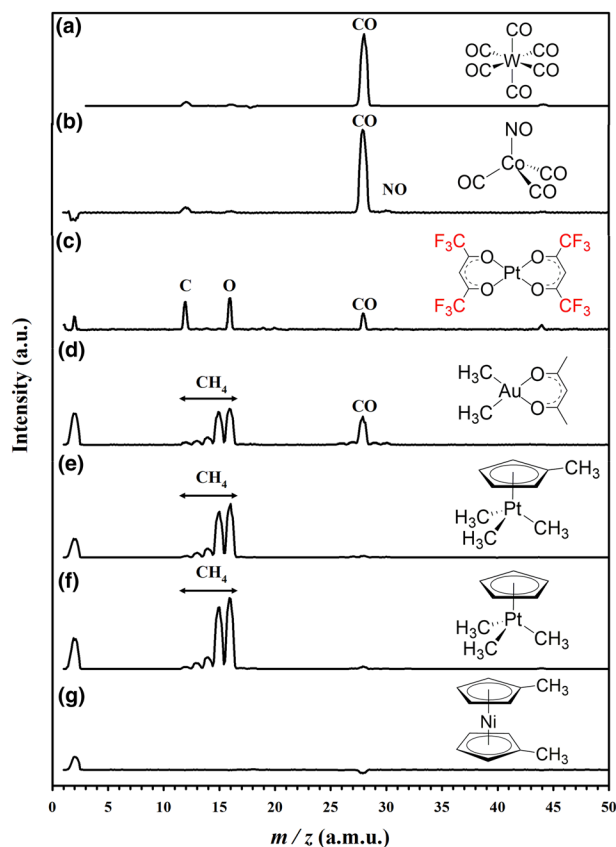
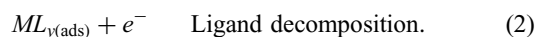
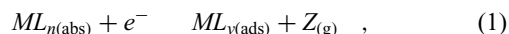


Figure 5. Mass spectrometry (MS) data for commercially available FEBID precursors adsorbed on a cold (<200 K) substrate and irradiated with 500 eV electrons. Precursors shown are: (a) $W(CO)_6$,^[38] (b) $Co(CO)_3NO$,^[39] (c) $Pt(hfac)_2$,^[40] (d) $Au(acac)Me_2$,^[41] (e) $MeCpPtMe_3$,^[25] (f) $CpPtMe_3$,^[25] and (g) $Ni(MeCp)_2$.^[26]

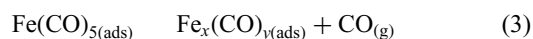
complex $[Pt(PF_3)_4]$. Since this is an inorganic precursor, it offers the obvious advantage of producing carbon-free deposits. However, FEBID nanostructures created from $Pt(PF_3)_4$ are typically found to contain phosphorus contamination.^[30,42,43] UHV surface science studies^[44] revealed that the decomposition of $Pt(PF_3)_4$ takes place in two sequential steps, analogous to the behavior of $W(CO)_6$. The first step involves electron-stimulated decomposition of the precursor, which leads to the desorption of one PF_3 ligand due to cleavage of a Pt–P bond. Further electron irradiation, however, results in the cleavage of P–F bonds in the remaining three PF_3 ligands, allowing desorption of fluoride anions, but retaining significant amounts of the remaining phosphorus as contamination.

The reactions of $W(CO)_6$ and $Pt(PF_3)_4$ reflect a sequential, two-step reaction sequence^[38,44,45] observed for several FEBID precursors that bear monodentate ligands: precursor decomposition accompanied by ligand desorption [Eq. (1)] followed by decomposition of the remaining ligands [Eq. (2)]. The organic contamination in FEBID nanostructures is a consequence of the second step of the reaction process, which is characterized by ligand decomposition, where ML_n indicates a

precursor composed of a metal (M) and ligands (L), and $Z_{(g)}$ represents volatile fragments desorbed.^[45]



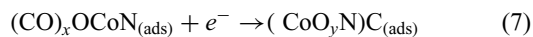
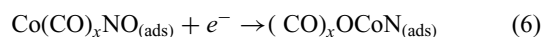
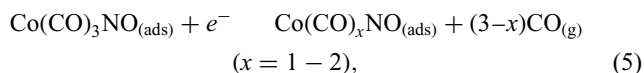
It should be noted that for a few precursors, the intermediates $[ML_{y(ads)}]$ formed by initial decomposition of the precursor have been shown to be unstable at room temperature and susceptible to further ligand desorption. Thermal ligand lability is relevant to practical FEBID, which is carried out in electron microscopes at or slightly above room temperature. Ligand lability at these temperatures has been demonstrated for the partially decarbonylated Fe_xCO_y intermediates produced by the electron-stimulated decomposition of $Fe(CO)_5$ [Eqs. (3) and (4)].^[31] This provides an explanation for the high metal content observed for FEBID nanostructures generated from $Fe(CO)_5$.



However, the best synthetic strategy remains to design precursors that will decompose to pure metals as a result solely of electron-stimulated reactions.

Monodentate ligands: heteroleptic complexes

An example of the reactivity of precursors that contain more than one ligand type is exemplified by a study performed on $Co(CO)_3NO$, a commonly used Co-containing FEBID precursor.^[39] Studies of $Co(CO)_3NO$ are consistent with electron irradiation initially resulting in the desorption of, on average, one to two CO ligands per molecule. After the initial CO desorption step, the remaining CO ligands are subjected to decomposition, resulting in a matrix of oxidized Co in an organic matrix. Thus, the behavior of the CO ligands is similar to that observed in $W(CO)_6$. In contrast, the NO ligands decompose to form a nitride species during the initial CO desorption step, reflecting a different reactivity for this ligand, despite the fact that NO^+ and CO are isoelectronic. The overall reactivity is summarized in Eqs. (5)–(7).



Chelating ligands: homoleptic complexes

More complex ligands are common in commercially available CVD precursors and several of these appear in FEBID studies.

These include bidentate chelating ligands, which occupy two coordination sites on the metal center, such as the hexafluoroacetylacetonate (hfac) ligand. Several common hfac-containing precursors including Pt(hfac)₂, Pd(hfac)₂, and Cu(hfac)₂ are capable of producing pure metallic films in CVD.^[46] However, in the FEBID process, nanostructures deposited from these precursors contain significant carbon contamination.^[47,48] UHV surface science studies of precursors containing bidentate chelating ligands found that the electron-simulated reactions are comprised of two steps, as seen for precursors containing exclusively monodentate ligands. However, the chemical reactions for these more complex precursors are less well-defined than for precursors that only contain simple monodentate ligands.^[40] Specifically, UHV surface science studies of Pt(hfac)₂, Pd(hfac)₂, and Cu(hfac)₂ revealed that in the first step, approximately 50% of oxygen and fluorine atoms desorb, along with a small amount of carbon. However, there is no loss of intact hfac ligands with carbon being lost in the form of CO (and possibly small amounts of CO₂), as determined by MS (see Fig. 5).^[40] Further electron beam irradiation of Pt(hfac)₂, Pd(hfac)₂, and Cu(hfac)₂ resulted in no further C or O loss, although fluorine continuously desorbed as F⁻ ions. This is a consequence of the susceptibility of C–F bonds to electron-stimulated decomposition, a process which causes the desorption of fluoride ions [C–F + e⁻ → C_(ads) + F_(g)⁻].^[49,50] Consequently, FEBID structures produced from Pt(hfac)₂, Pd(hfac)₂, and Cu(hfac)₂ are composed of metal atoms encased in an organic matrix, with little fluorine. A comparison of the chemical composition of films produced during the surface science studies with Pt(hfac)₂, Pd(hfac)₂, and Cu(hfac)₂ revealed that the nature of the metal center had relatively little effect on the overall composition of the final nanostructure.^[40] In the case of Cu(hfac)₂, a Cu–F species was observed, which led to an increased fluorine content in deposits created from Cu(hfac)₂; the analogous species was not observed with Pt and Pd.

Anionic polyhapto ligands

Another common ligand type is a polyhapto ligand, such as the cyclopentadienyl ligand (η^5 -C₅H₅ or Cp), which coordinates to the metal through adjacent atoms of a conjugated π system. The Cp ligand is found in one of the most widely used FEBID precursors, trimethyl methylcyclopentadienyl platinum (MeCpPtMe₃), which contains both monodentate methyl (CH₃ or Me) and polyhapto methylcyclopentadienyl (η^5 -MeCp₃) ligands. This precursor produces pure platinum films in CVD,^[51] but results in nanostructures with low platinum content, often <20%.^[30] The UHV surface science studies of MeCpPtMe₃ revealed that electron beam irradiation results in the cleavage of one of the three Pt–CH₃ bonds, leading to the desorption of methane, while the remaining two CH₃ ligands undergo subsequent electron-stimulated decomposition and the carbon atoms are incorporated into the deposit.^[25] Similar studies of adsorbed CpPtMe₃ demonstrated that CH₄ desorption is due to electron-stimulated cleavage of a Pt–CH₃

bond, rather than C–CH₃ bond cleavage in the MeCp ligand (see Fig. 5).^[25] In contrast, none of the carbon atoms in the polyhapto MeCp ligand desorb, and therefore all of them contribute to unwanted carbon contamination. Consequently, the Pt is encased in an amorphous carbon matrix (PtC_x film). Similarly, no carbon-containing species desorb when Ni(Cp)₂ is electron irradiated (see Fig. 5), and again, all of the carbon atoms in the Cp ligand contribute to the carbon contamination.^[26] The absence of any Cp or MeCp desorption is consistent with the behavior of bidentate chelating ligands such as hfac and acetoacetonate (acac).

General lessons on ligand choice from commercially available precursors

The UHV surface science results on commercially available CVD precursors described above show that there are structure-reactivity trends for different ligands that are preserved between different precursors. Under electron irradiation (Fig. 5), precursors containing multiple monodentate ligands (M–CO, M–PF₃, M–CH₃) desorb one or more of these ligands, although the remaining ligands undergo electron-stimulated decomposition. In contrast, anionic bidentate chelating and polyhapto ligands do not desorb as intact ligands, but rather decompose with the specific decomposition pathway dependent on the nature of the chelating or polyhapto ligand. Anionic polyhapto ligands such as cyclopentadienyl (η^5 -C₅H₅ or Cp) tend to be particularly problematic as the multiple metal–carbon bonds lead to ligand decomposition and carbon incorporation.

Beyond commercial precursors: complexes designed for FEBID (η^3 -allyl)ruthenium tricarbonyl halides

Studies on the heteroleptic complexes (η^3 -C₃H₅)Ru(CO)₃X (X = Cl, Br)^[52] were initially designed to address an interesting question raised by the results from the surface science studies on the Pt precursor MeCpPtMe₃.^[25] Under electron irradiation, the carbons of the anionic polyhapto ligand η^5 -MeCp (Fig. 6), which has five equivalent metal–carbon bonds, were incorporated into the deposit as carbon contamination. In contrast, one of the monodentate methyl groups, whose κ^1 bonding mode indicates one metal–carbon bond, was removed in an electron-induced process. Left unanswered was the question of how many metal–carbon bonds to a single ligand could be broken under FEBID conditions. The η^3 -allyl moiety of (η^3 -C₃H₅)Ru(CO)₃X, with its bonding mode involving three carbons provided an intermediate case. Another unexplored feature of these complexes is the metal–halogen bond. The halides in these complexes are directly bonded to the metal center, unlike in previously discussed precursors such as Pt(PF₃)₄ and the hfac complexes, where the fluorines are incorporated into a ligand. This compound also contains CO ligands, which had been previously demonstrated to be labile under FEBID conditions. The presence of three ligand types, η^3 -allyl, halide, and CO, in a single coordination sphere allows the evaluation of relative reactivity of the ligands as well.

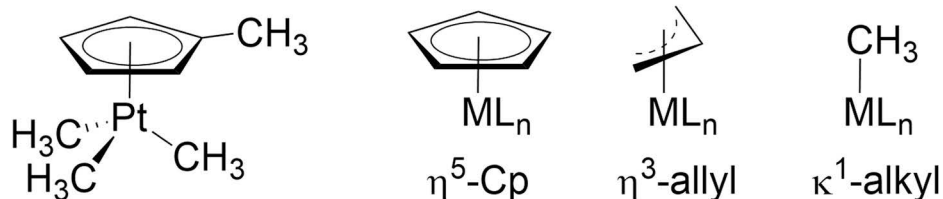


Figure 6. Metal-carbon bonding modes in organometallic complexes.

Under the UHV surface science conditions for electron-induced decomposition of the precursor, multiple CO ligands desorb but all of the carbon atoms in the η^3 -allyl (η^3 -C₃H₅) ligand are retained in the deposits.^[52] Facile loss of CO is consistent with the results of studies on gas-phase electron-molecule interactions of (η^3 -C₃H₅)Ru(CO)₃Br.^[53] Thus, anionic polyhapto ligands, even small ones, appear to be problematic for FEBID. Although the Br atoms do not desorb as the precursor decomposed, they can be removed from the film after exposure to higher electron doses as a result of a slower, electron-stimulated desorption process. Comparative studies with (η^3 -C₃H₅)Ru(CO)₃Cl reveal that the identity of the halogen does not influence the elementary reaction steps involved in the decomposition process.

UHV surface science modeling: platinum precursors

In the rational design of Pt precursors, the coordination spheres of the common oxidation states of Pt, Pt(0), Pt(II), and Pt(IV) have been considered. For Pt(0) and Pt(II) compounds, four-coordinate complexes are most common (Fig. 7).^[54] With Pt(0), the common formula is PtL₄ with four neutral ligands *L* while Pt(II) favors PtL₂X₂ complexes with two neutral ligands *L* and two negatively charged ligands *X*. In contrast, Pt(IV) compounds tend to be six-coordinate (note that the η^5 -Cp ligand occupies three coordination sites, so that MeCpPtMe₃

has six-coordinate pseudo-octahedral geometry).^[54] Based on our basic rules for the design of FEBID precursors to minimize the contamination from ligand fragments, the four-coordinate Pt(0) or Pt(II) complexes with fewer ligands would be more suitable for FEBID than the six-coordinate Pt(IV) compounds. However, there may be an upper limit to the number of *L*-type ligands that should be included in an optimal precursor, suggested by the studies of the electron-induced reactivity of Pt(PF₃)₄.^[30,42–44]

Collectively, our experimental observations and insights suggest that organometallic precursors with a small number of CO and halogen ligands could be used to generate deposits in FEBID with significantly higher metal concentrations (and correspondingly lower levels of organic contamination) compared with existing FEBID precursors. These considerations led us to explore the Pt(II) compound *cis*-Pt(CO)₂Cl₂ as a potential FEBID precursor.^[55] Studies of the electron-induced reactions of a few MLs of *cis*-Pt(CO)₂Cl₂ under UHV surface science conditions demonstrated that more than one of the CO ligands desorbed during the initial electron irradiation. Higher electron doses resulted in the complete loss of the Cl. When the steady-state deposition conditions of FEBID were simulated by creating ≈ 200 nm-thick deposits from *cis*-Pt(CO)₂Cl₂ in an Auger spectrometer on a room temperature substrate, the resulting material had the composition PtCl₂ and the Cl could not be removed by post-deposition electron beam processing.^[55,56] The absence of any carbon or oxygen contamination supports the idea that both of the CO ligands desorb from *cis*-Pt(CO)₂Cl₂ during FEBID. This lack of any carbon contamination is in contrast to the deposits formed from commercially available precursors such as MeCpPtMe₃ and Pt(hfac)₂,^[4,40] and is an important result due to the difficulty of removing carbon during post-deposition processing. The inability to remove the chlorine from the deposits created by FEBID in the Auger spectrometer was found to be a consequence of the limited escape depth of the chloride ions produced by electron interactions with PtCl₂.^[56] This effectively limits the depth of purification to nanostructures on the order of a few nanometers in size, including the ML films studied in the surface science experiments.

The Pt(II) complex cisplatin, *cis*-PtCl₂(NH₃)₂, has also been examined as a potential precursor for FEBID.^[57] The tendency of NH₃ ligands to form intermolecular hydrogen bonds results in low volatility for cisplatin, but its reactivity under electron

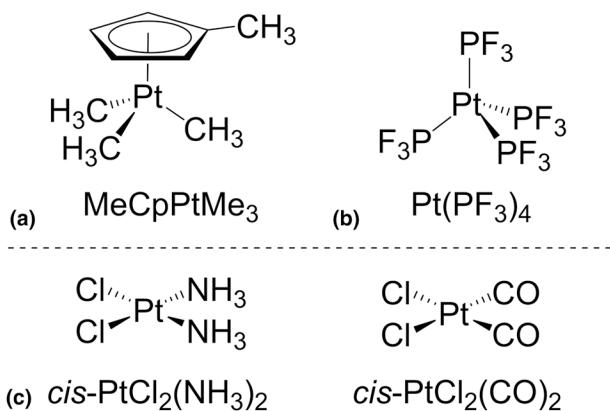


Figure 7. Platinum FEBID precursors with different formal oxidation states. (a) Pt(IV), (b) Pt(0), (c) Pt(II).

flux has been explored in several ways, allowing NH_3 to be evaluated as a ligand for FEBID precursors. Gas-phase dissociative electron attachment (DEA) studies on cisplatin demonstrated that NH_3 could be removed under electron irradiation at 5.5 eV.^[58] Consistent with the expectations from gas-phase studies, when $\text{cis-PtCl}_2(\text{NH}_3)_2$ particles were exposed to 20 keV electrons, the NH_3 ligands were rapidly removed, followed by a slower loss of chlorine.^[57] In contrast, FEBID structures created from $\text{cis-PtCl}_2(\text{NH}_3)_2$ formed deposits with a stoichiometry of PtCl, but the composition remained invariant to post-deposition electron exposure. Collectively, these results point to the facile loss of the two NH_3 ligands, analogous to the behavior of the CO ligands in $\text{cis-Pt}(\text{CO})_2\text{Cl}_2$.^[57] The loss of chlorine from $\text{cis-PtCl}_2(\text{NH}_3)_2$ particles was used to suggest that NH_3 can act as a reducing agent by decomposing under electron irradiation to produce species that facilitate the loss of Cl as HCl. This assertion is supported by the observation that atomic hydrogen, a species likely to be produced as a result of electron-stimulated NH_3 decomposition, efficiently removes Cl from PtCl_2 deposits.^[56,59] The presence of Cl in the deposits created in FEBID experiments was attributed to the ease with which NH_3 and/or its decomposition products could desorb from the growth surface during the deposition process, compared with the situation where a $\text{cis-PtCl}_2(\text{NH}_3)_2$ particle was exposed.^[57] The inability of post-deposition electron irradiation to change the PtCl composition of FEBID structures created from $\text{cis-PtCl}_2(\text{NH}_3)_2$ can be rationalized by the same limited purification depth observed for PtCl_2 deposits created from $\text{cis-Pt}(\text{CO})_2\text{Cl}_2$.^[56]

Control of precursor volatility by ligand selection: gold precursors

The need to deliver gas-phase precursor to the substrate for FEBID makes precursor volatility a crucial aspect in precursor design. We have used gold complexes as a platform to explore ligand effects on precursor volatility because of the high level of interest in the fabrication of gold nanostructures by FEBID. Nanostructures of Au have been shown to exhibit high DC conductivity and low ohmic losses, making them an ideal material for plasmonic applications.^[60] The ability of FEBID to fabricate nanostructures with 3D control makes

gold precursors of interest to enable the production of plasmonic structures. Classic examples of FEBID precursors used to fabricate gold nanostructures are β -diketonate-derived Au(III) complexes (Fig. 8, top). These CVD precursors are predominantly used because of their commercial availability and sufficient volatility for gas-phase transport in a gas injection system (GIS). In fact, these precursors produce pure gold films in CVD.^[61] However, complete desorption of the bidentate anionic acac ligand was not observed during electron-stimulated reactions of $\text{Au}(\text{acac})\text{Me}_2$ in UHV surface science studies, consistent with the general behavior of bidentate ligands in FEBID.^[41] As would be predicted from the results of that experiment, FEBID from the Au(III) acac precursors generally produces deposits consisting of a carbonaceous matrix embedded with sparse amounts of gold metal. The low gold content (≤ 20 , ≤ 40 , and ≤ 3 at.% for the acac,^[36,62] tfac,^[37,62–64] and hfac^[65] complexes, respectively), with the remainder of the deposit consisting of ligand-derived impurities, greatly hinders their application as optimal gold FEBID precursors.

As an alternative to the Au(III) precursors mentioned above, Cl–Au– PF_3 has been used to produce Au nanodeposits through FEBID.^[66–69] This was the first example of a precursor composed of Au(I) coordinated by inorganic, rather than carbon-rich ligands like those commonly found in CVD precursors. In terms of precursor design, this purely inorganic precursor offered a means to prevent carbon incorporation in the deposit. Notably when Cl–Au– PF_3 was used as an FEBID precursor, deposits consisted of pure metallic gold grains, a result that was in stark contrast to the deposits created from the traditional Au(III) precursors. Following a similar logic, the analogous carbon monoxide adduct Cl–Au–CO has also been used as an FEBID precursor.^[70] Similar results were obtained when this precursor was used in FEBID with deposit compositions consisting of >95 at.% Au with the remainder carbon.^[71]

Although Cl–Au– PF_3 and Cl–Au–CO [Fig. 8(b)] have drawn significant interest within the FEBID community, both Au(I) precursors suffer from moisture sensitivity^[70,72,73] and thermal instability.^[73–75] These compounds decompose at relatively low temperatures (RT for $L=\text{CO}$, 40–45 °C for $L=\text{PF}_3$)^[45,74,76] making storage and scale-up problematic for

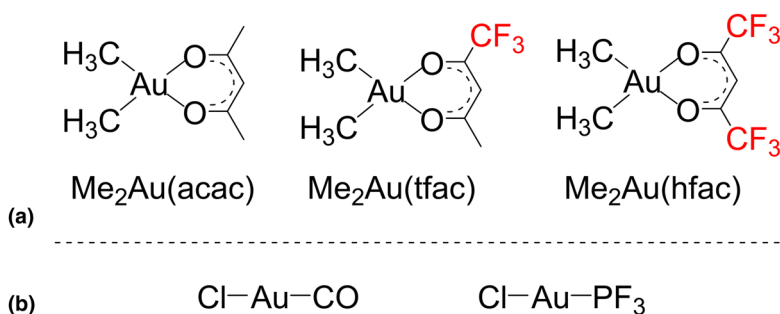
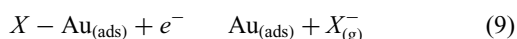
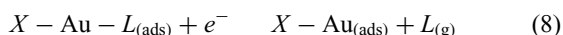


Figure 8. Gold FEBID precursors with different formal oxidation states. (a) Au(III), (b) Au(I).

FEBID. Additionally, Cl–Au–CO readily undergoes decarbonylation, making vacuum-based delivery of intact precursor molecules challenging. Evidence for decarbonylation in the GIS during FEBID is found in the studies of Cl–Au–CO, in which an initial pressure spike was noted as the GIS was opened to introduce gaseous precursor.^[71] The spike was attributed to a release of carbon monoxide, which had built up inside the reservoir. A mixture of Au and AuCl, which had not volatilized, was subsequently observed in the reservoir when the instrument was dismantled following the deposition.

Neither Cl–Au–PF₃ nor Cl–Au–CO is viable for practical use because their sensitivity toward temperature, air, moisture, and light renders both unsuitable for storage and scale-up to the quantities needed for industrial application.^[71] However, their structural and electronic similarity provides a starting point for precursor design. Structurally, the Au(I) precursors are advantageous, presenting a two-coordinate geometry in contrast to the existing Au(III) precursors that are four-coordinate. When there are fewer ligands coordinated to gold, less ligand material needs to be removed upon electron bombardment during FEBID, potentially affording lower levels of ligand-derived contamination in the deposits. These precursors are of the structural type *X*–Au–*L*, with one anionic ligand (*X*) and one neutral two-electron donor ligand (*L*). Both of these ligand types are preferred over chelating and polyhapto ligands, which often undergo ligand decomposition rather than complete desorption (*vide supra*). A general mechanism for the decomposition of *X*–Au–*L* complexes under FEBID conditions is proposed in Eqs. (8) and (9).^[45] Initially, the adsorbed precursor is exposed to the electrons whereupon the neutral *L* ligand desorbs from the surface forming gaseous *L* while an *X*–Au motif remains adsorbed on the surface. Subsequently, the anionic *X* ligand is ejected into the gas phase upon further irradiation of the partially decomposed *X*–Au species, resulting in a pure gold deposit.



In an attempt to find Au(I) precursors with higher stability, new complexes, including Me–Au–PMe₃, Cl–Au–PMe₃, and Cl–Au–SMe₂, were examined as potential FEBID precursors.^[76] Compared with Cl–Au–PF₃, decreasing the electronegativity of the substituents on the phosphine ligand improves the stability of the corresponding complexes in two ways. First, the sensitivity of the ligand to hydrolysis is minimized. Second, the basicity of the phosphorus is increased when the substituents are less electronegative, providing a stronger Au–*L* bond. Since the π backbonding in Cl–Au–CO is negligible,^[54,72] as is also likely for Cl–Au–PF₃, the strength of the Au–*L* interaction is a function of the σ donor strength of *L*.

Although the PMe₃ and SMe₂ complexes were stable under ambient conditions, an improvement over Cl–Au–PF₃ and Cl–

Au–CO, attempts to volatilize these precursors led to varying results. Notably, Me–Au–PMe₃ demonstrated sufficient thermal stability during volatilization, which resulted in the delivery of intact precursor molecules. However, the same was not true for Cl–Au–PMe₃, which decomposed before reaching the gas phase. This suggests that the identity of the *X* ligand in *X*–Au–*L* precursors is critical for successful precursor transport.

Effective utilization of *X*–Au–*L* complexes will require an understanding of their volatility trends, which led to a study of the effects of halide variation on the volatility of complexes in this series.^[77] This trend was examined for the *X*–Au–*L* (*X* = Cl, Br, I) complexes for several ligands [*L* = CN^tBu, CNMe, PMe₃, P(NMe₂)₃, P(OCH₂CF₃)₃]. The solid-state structures of Au(I) complexes are in part determined by aurophilic interactions, Au–Au bonds between individual molecules that can lead to aggregation in the solid. Volatilization of the precursors will involve breaking these intermolecular interactions. As a consequence, Au(I) complexes with smaller aggregation sizes and longer Au–Au bonds require less energy to volatilize and are thus promoted into the gas phase at lower temperatures as shown in Fig. 9 and Table 1. Within each series of isocyanide complexes, the onset temperature for sublimation (*T*_{sub}) decreased as the halide was varied from Cl → Br → I. For the phosphine and phosphoramidate complexes, the chloride and bromide have similar *T*_{sub} values with the bromide slightly higher but the iodide complex was again the most volatile of the three. For all the series of halide complexes, the iodide was most volatile due to its larger size, which precluded the formation of short Au–Au bonds and large aggregations. Although the thermal stability of Au(I) bromide and iodide complexes is lower than that of the analogous chlorides, the thermal decomposition temperatures of the *X*–Au–*L* complexes in the volatility study were significantly higher than their sublimation temperatures at 125 ± 1 mTorr, consistent with the isolation of clean precursor by sublimation.

A complementary study of Au(I) complexes including both experiment and calculations further supports the concept that solid-state aurophilic interactions influence the stability and volatility of Au(I) complexes.^[86] Notably, these results suggest that the instability of Cl–Au–CO arises from aurophilic bonding in the solid lattice, which is not present in the gas phase. Density functional theory (DFT) calculations suggest that the decarbonylation of a lattice of Cl–Au–CO molecules is more facile than the decarbonylation of single Cl–Au–CO molecules.^[86] In the context of this result, FEBID from this precursor (*vide supra*) is likely a result of the volatilization of a small quantity of intact molecules, while the bulk of the precursor decomposes, resulting in a burst of CO pressure inside the instrument and AuCl in the precursor crucible.

The same study also rationalized the different volatilities of *X*–Au–PMe₃ complexes (*X* = Cl and Me),^[86] a result that had been noted by the authors in a previous publication.^[76] The crystal structure of the Me complex has longer Au–Au distances, which form dimeric structures with Au–Au distances

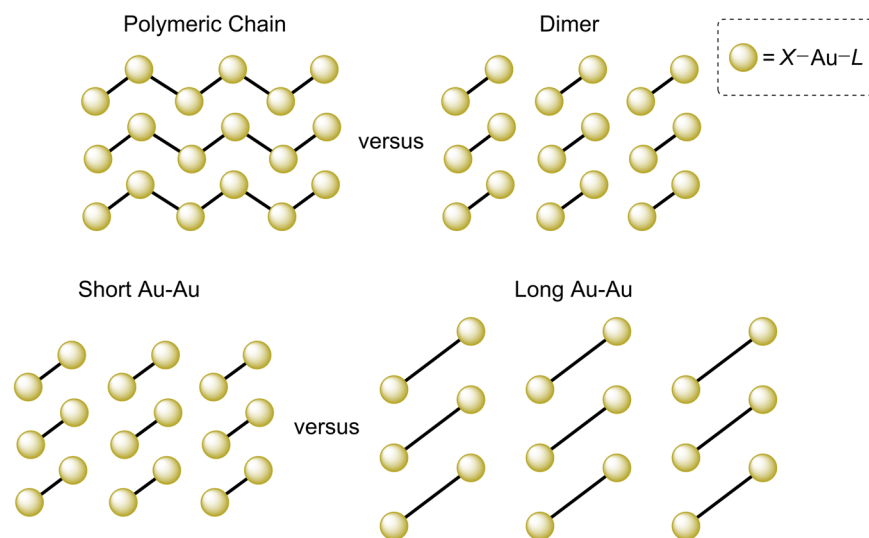


Figure 9. Relationship between $X\text{-Au-L}$ volatility and the nature of aurophilic bonding.

of 3.3130(4) and 3.4073(5) Å with negligible Au–Au interactions for the remaining molecules in the unit cell.^[86] In contrast, the Cl complex forms longer Au–Au bonds and forms larger

aggregates in the solid state (Table 1). The decreased Au–Au bonding in the Me complex explains its volatility under vacuum relative to the non-volatile chloride.^[86]

Table 1. Variation in onset temperature for sublimation at 125 ± 1 mTorr (T_{sub}) with Au–Au bonding.^[77]

	Identity of X	T_{sub} (°C)	Au–Au length (Å)	Aggregation type	Structure reference
$X\text{-Au-CN}^t\text{Bu}$	Cl	64	3.695(1)	Polymeric chain	[78]
	Br	53	3.689(1)	Polymeric chain	[79]
	I	51	4.612(3)	Dimer	[80]
$X\text{-Au-CNMe}$	Cl	83	3.637(1), [3.442 ^a], [2.69 ^b]	Polymeric chain [dimer ^{a,b}]	[79–81]
	Br	79	[2.70 ^b]	[Dimer ^b]	[81]
	I	65	[3.792 ^a], [2.72 ^b]	[Dimer ^{a,b}]	[80,81]
$X\text{-Au-PMe}_3$	Cl	78	3.648(1), 3.548(2)	Polymeric chain	[82]
	Br	83	3.271(1), 3.356(1), 3.386(1)	Trimer	[83]
	I	70	3.168(1)	Dimer	[84]
$X\text{-Au-P(NMe}_2)_3$	Cl	69	6.816	Monomer	[85]
	Br	73	6.8105(2)	Monomer	[77]
	I	62	6.9198(3)	Monomer	[77]
$X\text{-Au-P(OCH}_2\text{CF}_3)_3$	Cl	55	3.0611(3), 3.2188(3), 3.1584(3)	Tetramer	[77]
	Br	73	3.0850(17), 3.1074(15), 3.1157(15), 3.1277(17)	2 monomers + 2 trimers	[77]
	I	56	3.1251(4)	Dimer	[77]

Entries denoted with square brackets [] are to emphasize the following theoretical contributions:

^aMP2 calculations on antiparallel dimers ($X\text{-Au-CNMe}$)₂.

^bDFT calculations on antiparallel dimers ($X\text{-Au-CNMe}$)₂.

Control of stoichiometry in alloys: heterobimetallic precursors

The scope of materials that can be deposited by FEBID has progressed to include mixed metal alloys^[87–89] and also metal–silicon^[90,91] and metal–carbon alloys.^[92] In principle, FEBID of nanoalloys with controlled composition is an attractive target because their materials properties could be tailored for specific applications. In addition to composition, the size and shape of alloys govern their magnetic properties^[93] and these properties can be controlled in FEBID. Initial reports on the deposition of nanoalloys by FEBID utilize a co-deposition method in which two different monometallic precursors are introduced simultaneously.^[89] Control of the deposit stoichiometry in co-reactant systems can be challenging. Co-deposition requires a modified electron microscope setup, incorporating multiple GIS that simultaneously introduce each precursor required to make the desired alloy. Since this technique requires multiple precursors, preliminary experiments are often required to determine the growth rate from each precursor to optimize their respective precursor flux.^[87,89] An additional factor that governs the deposit compositions is the differences in the kinetics of adsorption and dissociation of each precursor to the substrate.^[92]

Single-source precursors that contain multiple metal centers offer the advantage of reproducible control over deposit stoichiometry since each metal atom originates from the same precursor molecule. Polynuclear clusters and heterobimetallic complexes have been used as single-source precursors in

CVD to successfully grow mixed metal alloys and oxides.^[94–99] More recently, heterobimetallic single-source precursors have been used in FEBID. A notable example is the heterometallic cluster $\text{HFeCo}_3(\text{CO})_{12}$ (Fig. 10), which produces high-purity deposits of >80 at.% FeCo when used for FEBID nanofabrication.^[100] It is also important to note that the deposits retained the stoichiometry of the FeCo_3 metal core of the precursor. The high-purity deposits from $\text{HFeCo}_3(\text{CO})_{12}$ exhibited ferromagnetism, making them attractive for magnetic data storage applications. The magnetism result is important because this property can be negatively affected by the low metal content of FEBID deposits.

In contrast to the behavior of $\text{HFeCo}_3(\text{CO})_{12}$, the similar cluster $\text{H}_2\text{FeRu}_3(\text{CO})_{13}$ (Fig. 8) affords FEBID deposits with relatively low (<25%) metal contents.^[101] X-ray crystallographic determination^[101–103] of the structure of the FeRu_3 cluster indicated that the absence of a bridging CO ligand on one Fe–Ru bond axis gives rise to an extended bond length. Likewise, the Ru–Ru bonds with hydride bridges are longer than the unbridged counterpart. Together, these contribute to the distortion from the idealized tetrahedral core structure of $\text{HFeCo}_3(\text{CO})_{12}$. UHV surface science studies revealed that both $\text{HFeCo}_3(\text{CO})_{12}$ and $\text{H}_2\text{FeRu}_3(\text{CO})_{13}$ react in a two-step process, analogous to the reactions of monometallic precursors.^[101,104] For both bimetallic precursors, the initial electron-stimulated decomposition step is similar, resulting in the desorption of a significant and similar number (8–9) of CO groups to form partially decarbonylated intermediates.^[101,104]

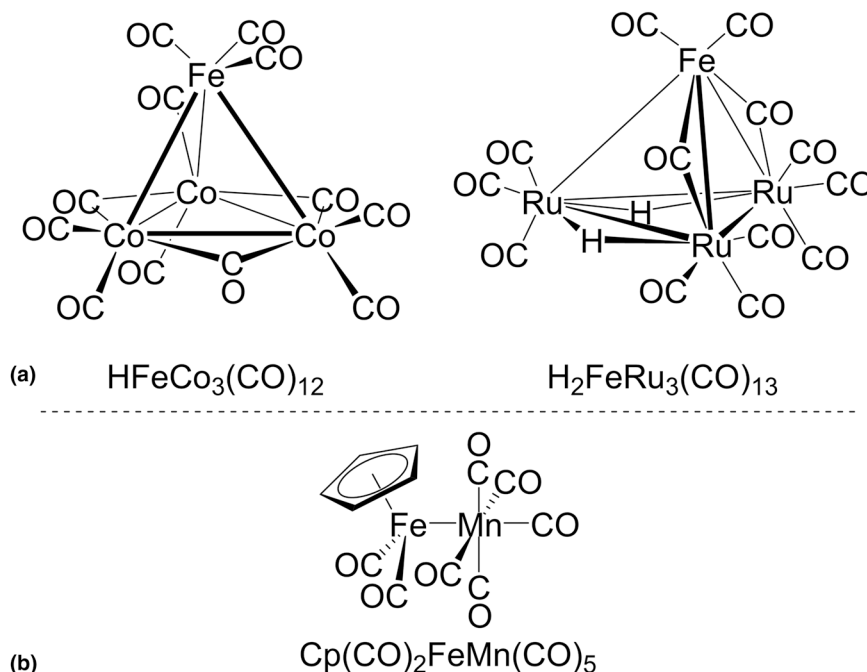
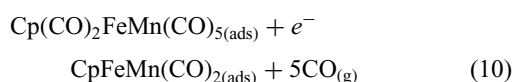


Figure 10. (a) Tetranuclear heterometallic clusters and (b) heterobimetallic complex studied as precursors for FEBID of alloys. The $\mu^3\text{-H}$ in $\text{HFeCo}_3(\text{CO})_{12}$ is omitted for clarity.

Comparisons with related gas-phase studies suggests that the electron-stimulated decomposition of these two bimetallic precursors proceeds through dissociative ionization (DI).^[101,104] The critical difference between $\text{H}_2\text{FeRu}_3(\text{CO})_{13}$ and $\text{HFeCo}_3(\text{CO})_{12}$ appears to lie in the stability of the partially decarbonylated intermediate. In the case of $\text{HFeCo}_3(\text{CO})_{12}$, the partially decarbonylated intermediate generated from initial electron-induced decomposition undergoes complete CO desorption when annealed to RT, which is consistent with the high metal content obtained in steady-state FEBID experiments.^[100,104] This is not the case with $\text{H}_2\text{FeRu}_3(\text{CO})_{13}$, where the partially decarbonylated intermediate is relatively stable toward additional electron flux and thermal processing.^[101,104] The reactivity differences between $\text{HFeCo}_3(\text{CO})_{12}$ and $\text{H}_2\text{FeRu}_3(\text{CO})_{13}$ demonstrate that the nature and reactivity of the intermediate species produced as a result of precursor decomposition are critically important in determining the ultimate metal content achieved in FEBID.

The influence of the coordination sphere, including metal–metal bonding, in bimetallic precursors during electron beam-induced decomposition is not yet understood, despite studies of the cluster complexes $\text{HFeCo}_3(\text{CO})_{12}$ and $\text{H}_2\text{FeRu}_3(\text{CO})_{13}$. In an effort to elucidate electronic structure effects, studies were carried out on $\text{Cp}(\text{CO})_2\text{FeMn}(\text{CO})_5$, a bimetallic precursor with a simpler structure.^[105] Structurally, $\text{Cp}(\text{CO})_2\text{FeMn}(\text{CO})_5$ is different than the clusters $\text{HFeCo}_3(\text{CO})_{12}$ and $\text{H}_2\text{FeRu}_3(\text{CO})_{13}$. In $\text{Cp}(\text{CO})_2\text{FeMn}(\text{CO})_5$, the metal centers are held together by a single unsupported metal–metal bond. There are no bridging CO or hydride ligands to complicate the metal–metal bonding. Each metal center has a different set of ancillary ligands consisting of $\eta^5\text{-Cp}$ and CO on the Fe fragment and CO only on Mn (Fig. 8, bottom).

In surface science studies with $\text{Cp}(\text{CO})_2\text{FeMn}(\text{CO})_5$, initial electron-induced decomposition of thin films of the precursor resulted in facile CO desorption, producing a partially decarbonylated surface-bound intermediate.^[105] During this stage of the decomposition, approximately five CO ligands are desorbed per precursor molecule [Eq. (10)]. For higher electron doses, the film composition remains unchanged, but ligand decomposition is initiated as seen for other FEBID precursors. During this process, the remaining CO ligands are decomposed, forming graphitic carbon and reactive oxygen species (ROS) that effect Mn oxidation [Eqs. (10)–(12)]. In contrast to the behavior of Mn atoms, the bonding environment of Fe remains relatively unchanged throughout the course of electron irradiation [Eq. (12)].



Consistent with the results from other complexes bearing anionic polyhapto ligands, no desorption of the cyclopentadienyl carbons was observed, resulting in the incorporation of the carbon atoms as impurities in the deposit. It is interesting that during the electron-stimulated decomposition of CO, oxidation occurred at Mn rather than Fe. If the CO loss occurs predominantly from the $\text{Mn}(\text{CO})_5$ moiety [Eq. (8)], it is reasonable to expect that the formation of empty coordination sites would provide facile access of ROS to the metal center, enabling oxidation as observed. The absence of Fe oxidation may be a result of the Cp ligand acting as a protecting group, forming a carbonaceous shell around the Fe center, which prevents reactivity with the ROS. These studies with $\text{Cp}(\text{CO})_2\text{FeMn}(\text{CO})_5$ suggest that rational manipulation of the coordination sphere of each metal center could be used to control the electron-induced chemistry of precursors incorporating multiple metal atoms.

An interesting facet of the gas-phase electron–molecule interactions of $\text{Cp}(\text{CO})_2\text{FeMn}(\text{CO})_5$ is the qualitative relationship between the DI studies carried out with 70 eV electrons^[106] and the behavior of the precursor under UHV surface science conditions.^[105] Because electron impact mass spectrometry (EI-MS) with incident electrons of similar energy is a standard characterization tool in synthesis laboratories, the DI (or EI-MS) behavior of potential precursors could be used for the pre-screening of precursors by synthetic chemists before more extensive studies of electron–molecule interactions under FEBID conditions are undertaken. The use of MS for the pre-screening of precursors is a common practice in the CVD community, with the understanding that care during interpretation of the data is warranted because MS detects ionized species while thermal decomposition during CVD is more likely to produce neutral fragments.^[107,108] In FEBID, the precursor is decomposed by electron–molecule interactions so the relationship between EI-MS and FEBID is expected to be closer than in CVD. In the case of $\text{Cp}(\text{CO})_2\text{FeMn}(\text{CO})_5$, the DI (EI-MS) data do resemble the UHV surface science results. In the gas-phase electron–molecule interaction studies, the highest intensity DI peaks ($[\text{CpFe}]^+$, $[\text{CpFe}(\text{CO})_2]^+$, $[\text{CpFeMn}(\text{CO})_2]^+$, and $[\text{CpFeMn}(\text{CO})]^+$) still contain the Cp ligand,^[106] consistent with the persistence of the Cp carbons under electron irradiation in the UHV surface science experiments.^[105] Significant intensity of peaks for various combinations of CO loss in the DI spectrum is reflected in loss of those ligands from the surface.

However, despite the relationship between EI-MS and FEBID, interpretative caution is still in order because FEBID has features that are not present in the gas-phase electron–molecule interactions of EI-MS. One important difference is that in FEBID, precursor molecules are exposed to a range of secondary electrons from the substrate rather than the single-electron energy (≈ 70 eV) commonly used in EI-MS, and ion yields are known to depend on the incident electron energy.^[109] Perhaps more importantly, precursors can decompose as a result of several different types of electron–molecule interactions, of which DI is only one.^[110] In particular, low-energy

secondary electrons (typically <10 eV) can initiate decomposition as a result of DEA. Previous comparisons between single-collision gas-phase studies where the incident energy can be tuned and UHV surface science data suggest that some precursors decompose principally by DEA and some by DI.^[29] Another caveat with EI-MS is that it can only measure the initial electron interactions with the precursor molecule, while secondary electron processes associated with adsorbed intermediates also play an important role in determining the ultimate composition of the deposit formed in FEBID. For example, in the case of Cp(CO)₂FeMn(CO)₅, the oxidation of Mn after the decomposition of CO on the surface^[105] cannot, of course, be anticipated from the DI spectra. However, the critical point for pre-screening purposes is that the facile CO ligand loss pathways on the surface and the persistence of the Cp ligand can be seen in the DI. If these types of insights turn out to be generalizable across a range of different precursors, EI-MS could be of great utility in pre-screening precursors before their electron-induced surface reactions are studied or FEBID is attempted.

Conclusions and outlook

During FEBID, UHV surface science studies have revealed that the initial electron-stimulated decomposition of adsorbed precursor molecules is accompanied by ligand desorption from the organometallic complex to form a surface-bound intermediate. Subsequent electron irradiation of this intermediate decomposes the remaining ligands (unless they are unstable toward desorption at room temperature), with the exception of halogen atoms, which can desorb via an electron-stimulated desorption process.

To minimize organic contamination in organometallic precursors designed for use in FEBID, our results suggest a number of guiding principles should be followed:

- (1) Organometallic precursors with a small number of monodentate ligands are desirable as FEBID precursor candidates.
- (2) Among the monodentate ligands studied, CO and NH₃ groups appear to be privileged as they preferentially desorb in mixed ligand complexes and it is common for multiple CO or NH₃ ligands to desorb. However, the tendency of NH₃ ligands to undergo intermolecular hydrogen bonding may cause problems with precursor volatility.
- (3) Anionic ligands bonded through multiple coordination sites (bidentate, polydentate, or polyhapto) should be avoided. Anionic polyhapto carbon ligands such as cyclopentadienyl (η^5 -C₅H₅) or allyl (η^3 -C₃H₅) tend to be particularly problematic as the multiple metal–carbon bonds lead to ligand decomposition and carbon incorporation.
- (4) Halogen atoms attached directly to late transition metal centers do not desorb during initial precursor decomposition but can be removed subsequently under the influence of higher doses of electrons.
- (5) Precursors must be sufficiently volatile for transport in a GIS at temperatures <100 °C. We find that the onset

temperature for sublimation of a precursor provides a practical surrogate for vapor pressure.

In comparison to monometallic FEBID precursors, development of general designs for heterobimetallic precursors is anticipated to be challenging because unsupported metal–metal bonds tend to be weak. The lability of these bonds combined with decreased precursor volatility arising from higher molecular weights is likely to cause difficulties in volatilizing the compounds without decomposing them. Nonetheless, combining precursor design with UHV surface science studies and gas-phase electron–molecule interactions will continue to provide insights for use in precursor design for FEBID.

Acknowledgments

D.H.F. and L.M.W. thank the National Science Foundation for support of this work through the linked collaborative grants CHE-1607621 and CHE-1607547. Support of preliminary studies was provided by the donors of the American Chemical Society Petroleum Research Fund (PRF Grant # 54519-ND5) and by FEI.

References

1. W. van Dorp, C. Hagen, P. Crozier, and P. Kruit: Growth behavior near the ultimate resolution of nanometer-scale focused electron beam-induced deposition. *Nanotechnology* **19**, 225305 (2008).
2. S.J. Randolph, J.D. Fowlkes, and P.D. Rack: Focused, nanoscale electron-beam-induced deposition and etching. *Crit. Rev. Solid State Mater. Sci.* **31**, 55 (2006).
3. W.F. van Dorp and C.W. Hagen: A critical literature review of focused electron beam induced deposition. *J. Appl. Phys.* **104**, 081301 (2008).
4. I. Utke, P. Hoffman, and J. Melngailis: Gas-assisted focused electron beam and ion beam processing and fabrication. *J. Vac. Sci. Technol. B* **26**, 1197 (2008).
5. M. Huth, F. Poratti, C. Schwalb, M. Winhold, R. Sachser, M. Dukic, J. Adams, and G. Fantner: Focused electron beam induced deposition: a perspective. *Beilstein J. Nanotechnol.* **3**, 597 (2012).
6. H. Acar: *Fabrication of plasmonic nanostructures with electron beam induced deposition* (University of Twente, Zutphen, 2013).
7. M. Gavagnin, H.D. Wanzenboeck, D. Belic, and E. Bertagnolli: Synthesis of individually tuned nanomagnets for nanomagnet logic by direct write focused electron beam induced deposition. *ACS Nano* **7**, 777 (2013).
8. J. Brown, P. Kocher, C.S. Ramanujan, D.N. Sharp, K. Torimitsu, and J.F. Ryan: Electrically conducting, ultra-sharp, high aspect-ratio probes for AFM fabricated by electron-beam-induced deposition of platinum. *Ultramicroscopy* **133**, 62 (2013).
9. K. Murakami and M. Takai: Characteristics of nano electron source fabricated using beam assisted process. *J. Vac. Sci. Technol. B* **22**, 1266 (2004).
10. K. Murakami and M. Takai: Nano electron source fabricated by beam-induced deposition and its unique feature. *Microelectron. Eng.* **132**, 74 (2015).
11. A. Perentes and P. Hoffmann: Focused electron beam induced deposition of Si-based materials from SiO_xC_y to stoichiometric SiO₂: chemical compositions, chemical-etch rates, and deep ultraviolet optical transmissions. *Chem. Vap. Deposition* **13**, 176 (2007).
12. K. Edinger, H. Becht, J. Bihl, V. Boegli, M. Budach, T. Hofmann, H.W. P. Koops, P. Kuschnerus, J. Oster, P. Spies, and B. Weyrauch: Electron-beam-based photomask repair. *J. Vac. Sci. Technol. B* **22**, 2902 (2004).
13. T. Liang, E. Frendberg, B. Lieberman, and A. Stivers: Advanced photolithographic mask repair using electron beams. *J. Vac. Sci. Technol. B* **23**, 3101 (2005).

14. C.T.H. Heerkens, M.J. Kamerbeek, W.F. van Dorp, C.W. Hagen, and J. Hoekstra: Electron beam induced deposited etch masks. *Microelectron. Eng.* **86**, 961 (2009).
15. B. Hubner, H.W.P. Koops, H. Pagnia, N. Sotnik, J. Urban, and M. Weber: Tips for scanning tunneling microscopy produced by electron-beam-induced deposition. *Ultramicroscopy* **42–44**, 1519 (1992).
16. I.-C. Chen, L.-H. Chen, C. Orme, A. Quist, R. Lal, and S. Jin: Fabrication of high-aspect-ratio carbon nanocone probes by electron beam induced deposition patterning. *Nanotechnology* **17**, 4322 (2006).
17. S. Graells, R. Alcubilla, G. Badenes, and R. Quidant: Growth of plasmonic gold nanostructures by electron beam induced deposition. *Appl. Phys. Lett.* **91**, 121112 (2007).
18. A. Weber-Bargioni, A. Schwartzberg, M. Schmidt, B. Harteneck, D.F. Ogletree, P.J. Schuck, and S. Cabrini: Functional plasmonic antenna scanning probes fabricated by induced-deposition mask lithography. *Nanotechnology* **21**, 065306 (2010).
19. H.W.P. Koops, O.E. Hoinkis, M.E.W. Honsberg, R. Schmidt, R. Blum, G. Bottger, A. Kuligk, C. Liguda, and M. Eich: Two-dimensional photonic crystals produced by additive nanolithography with electron beam-induced deposition act as filters in the infrared. *Microelectron. Eng.* **57–8**, 995 (2001).
20. J. Basu, D.B. Carter, R. Divakar, V.B. Shenoy, and N. Ravishankar: Modified electron-beam-induced deposition of metal nanostructure arrays using a parallel electron beam. *Appl. Phys. Lett.* **93**, 133104/1 (2008).
21. J.D. Fowlkes, R. Winkler, B.B. Lewis, M.G. Stanford, H. Plank, and P.D. Rack: Simulation-guided 3D nanomanufacturing via focused electron beam induced deposition. *ACS Nano* **10**, 6163 (2016).
22. R. Winkler, F.-P. Schmidt, U. Haselmann, J.D. Fowlkes, B.B. Lewis, G. Kothleitner, P.D. Rack, and H. Plank: Direct-write 3D nanoprinting of plasmonic structures. *ACS Appl. Mater. Interfaces* **9**, 8233 (2017).
23. L. McElwee-White, J. Koller, D. Kim, and T.J. Anderson: Mechanism-based design of precursors for MOCVD. *ECS Trans.* **25**, 161 (2009).
24. L. McElwee-White: Design of precursors for the CVD of inorganic thin films. *Dalton Trans.*, 5327 (2006).
25. J.D. Wnuk, J.M. Gorham, S.G. Rosenberg, W.F. van Dorp, T.E. Madey, C.W. Hagen, and D.H. Fairbrother: Electron induced surface reactions of the organometallic precursor trimethyl(methylcyclopentadienyl)platinum(IV). *J. Phys. Chem. C* **113**, 2487 (2009).
26. J.D. Wnuk, S.G. Rosenberg, J.M. Gorham, W.F. van Dorp, C.W. Hagen, and D.H. Fairbrother: Electron beam deposition for nanofabrication: insights from surface science. *Surf. Sci.* **605**, 257 (2011).
27. N. Silvis-Cividjian, C.W. Hagen, and P. Kruit: Spatial resolution limits in electron-beam-induced deposition. *J. Appl. Phys.* **98**, 084905 (2005).
28. A. Botman, D.A.M.D. Winter, and J.J.L. Mulders: Electron-beam-induced deposition of platinum at low landing energies. *J. Vac. Sci. Technol. B* **26**, 2460 (2008).
29. R.M. Thorman, T.P.R. Kumar, D.H. Fairbrother, and O. Ingolfsson: The role of low-energy electrons in focused electron beam induced deposition: four case studies of representative precursors. *Beilstein J. Nanotechnol.* **6**, 1904 (2015).
30. A. Botman, M. Hesselberth, and J.J.L. Mulders: Investigation of morphological changes in platinum-containing nanostructures created by electron-beam-induced deposition. *J. Vac. Sci. Technol. B* **26**, 2464 (2008).
31. M.A. Henderson, R.D. Ramsier, and J.T. Yates: Low-energy electron induced decomposition of Fe(CO)₅ adsorbed on Ag(111). *Surf. Sci.* **259**, 173 (1991).
32. R. Córdoba, J. Sesé, J.M. De Teresa, and M.R. Ibarra: High-purity cobalt nanostructures grown by focused-electron-beam-induced deposition at low current. *Microelectron. Eng.* **87**, 1550 (2010).
33. M. Weber, H.W.P. Koops, M. Rudolph, J. Kretz, and G. Schmidt: New compound quantum dot materials produced by electron-beam induced deposition. *J. Vac. Sci. Technol. B* **13**, 1364 (1995).
34. F. Porriati, R. Sachser, and M. Huth: The transient electrical conductivity of W-based electron-beam-induced deposits during growth, irradiation and exposure to air. *Nanotechnology* **20**, 195301 (2009).
35. P.D. Rack, S. Randolph, Y. Deng, J. Fowlkes, Y. Choi, and D.C. Joy: Nanoscale electron-beam-stimulated processing. *Appl. Phys. Lett.* **82**, 2326 (2003).
36. J.J.L. Mulders, L.M. Belova, and A. Riazanova: Electron beam induced deposition at elevated temperatures: compositional changes and purity improvement. *Nanotechnology* **22**, 055302 (2011).
37. H.W.P. Koops, R. Weiel, D.P. Kern, and T.H. Baum: High-resolution electron-beam induced deposition. *J. Vac. Sci. Technol. B* **6**, 477 (1988).
38. S.G. Rosenberg, M. Barclay, and D.H. Fairbrother: Electron induced reactions of surface adsorbed tungsten hexacarbonyl (W(CO)₆). *Phys. Chem. Chem. Phys.* **15**, 4002 (2013).
39. S.G. Rosenberg, M. Barclay, and D.H. Fairbrother: Electron beam induced reactions of adsorbed cobalt tricarbonyl nitrosyl (Co(CO)₃NO) molecules. *J. Phys. Chem. C* **117**, 16053 (2013).
40. S.G. Rosenberg, M. Barclay, and D.H. Fairbrother: Electron induced surface reactions of organometallic metal(hfac)₂ precursors and deposit purification. *ACS Appl. Mater. Interfaces* **6**, 8590 (2014).
41. J.D. Wnuk, J.M. Gorham, S.G. Rosenberg, W.F. van Dorp, T.E. Madey, C.W. Hagen, and D.H. Fairbrother: Electron induced irradiation of dimethyl-(acetylacetonate) gold(III) adsorbed onto solid substrates. *J. Appl. Phys.* **107**, 054301/1 (2010).
42. J.D. Barry, M.H. Ervin, J. Molstad, A. Wickenden, T. Brintinger, P. Hoffmann, and J. Meingailis: Electron beam induced deposition of low resistivity platinum from Pt(PF₃)₄. *J. Vac. Sci. Technol. B* **24**, 3165 (2006).
43. S. Wang, Y.M. Sun, Q. Wang, and J.M. White: Electron-beam induced initial growth of platinum films using Pt(PF₃)₄. *J. Vac. Sci. Technol. B* **22**, 1803 (2004).
44. K. Landheer, S. Rosenberg, L. Bernau, P. Swiderek, I. Utke, C. Hagen, and D.H. Fairbrother: Low-energy electron-induced decomposition and reactions of adsorbed tetrakis(trifluorophosphine)platinum [Pt(PF₃)₄]. *J. Phys. Chem. C* **115**, 17452 (2011).
45. J.A. Spencer, S. Rosenberg, M. Barclay, Y.-C. Wu, L. McElwee-White, and D.H. Fairbrother: Understanding the electron stimulated surface reactions of organometallic complexes to enable design of precursors for electron beam induced deposition. *Appl. Phys. A Mater. Sci. Process.* **117**, 1631 (2014).
46. N.L. Jeon, W. Lin, M.K. Erhardt, G.S. Girolami, and R.G. Nuzzo: Selective chemical vapor deposition of platinum and palladium directed by monolayers patterned using microcontact printing. *Langmuir* **13**, 3833 (1997).
47. A. Luisier, I. Utke, T. Bret, F. Cicoira, R. Hauert, S.W. Rhee, P. Doppelt, and P. Hoffmann: Comparative study of Cu-precursors for 3D focused electron beam induced deposition. *J. Electrochem. Soc.* **151**, C590 (2004).
48. H. Miyazoe, I. Utke, H. Kikuchi, S. Kiriu, V. Friedli, J. Michler, and K. Terashima: Improving the metallic content of focused electron beam-induced deposits by a scanning electron microscope integrated hydrogen-argon microplasma generator. *J. Vac. Sci. Technol. B* **28**, 744 (2010).
49. P.E. Laibinis, R.L. Graham, H.A. Biebuyck, and G.M. Whitesides: X-Ray damage to CF₃CO₂-terminated organic monolayers on Si/Au—principal effect of electrons. *Science* **254**, 981 (1991).
50. C.C. Perry, A.J. Wagner, and D.H. Fairbrother: Electron stimulated C-F bond breaking kinetics in fluorine-containing organic thin films. *Chem. Phys.* **280**, 111 (2002).
51. Z. Xue, M.J. Strouse, D.K. Shuh, C.B. Knobler, H.D. Kaesz, R.F. Hicks, and R.S. Williams: Characterization of (methylcyclopentadienyl)trimethylplatinum and low-temperature organometallic chemical vapor deposition of platinum metal. *J. Am. Chem. Soc.* **111**, 8779 (1989).
52. J.A. Spencer, J.A. Brannaka, M. Barclay, L. McElwee-White, and D.H. Fairbrother: Electron induced surface reactions of η^3 -allyl ruthenium tricarbonyl bromide $[(\eta^3\text{-C}_3\text{H}_5)\text{Ru}(\text{CO})_3\text{Br}]$: contrasting the behavior of different ligands. *J. Phys. Chem. C* **119**, 15349–15359 (2015).
53. R.M. Thorman, J.A. Brannaka, L. McElwee-White, and O. Ingolfsson: Low energy electron-induced decomposition of $(\eta^3\text{-C}_3\text{H}_5)\text{Ru}(\text{CO})_3\text{Br}$, a potential focused electron beam induced deposition precursor with a heteroleptic ligand set. *Phys. Chem. Chem. Phys.* **19**, 13264 (2017).

54. F.A. Cotton, G. Wilkinson, C. Murillo, and M. Bochmann: *Advanced Inorganic Chemistry*, 6th ed. (Wiley, New York, 1999).
55. J.A. Spencer, Y.C. Wu, L. McElwee-White, and D.H. Fairbrother: Electron induced surface reactions of cis-Pt(CO)₂Cl₂: a route to focused electron beam induced deposition of pure Pt nanostructures. *J. Am. Chem. Soc.* **138**, 9172 (2016).
56. J.A. Spencer, M. Barclay, M.J. Gallagher, R. Winkler, I. Unlu, Y.-C. Wu, H. Plank, L. McElwee-White, and D.H. Fairbrother: Comparing postdeposition reactions of electrons and radicals with Pt nanostructures created by focused electron beam induced deposition. *Beilstein J. Nanotechnol.* **8**, 2410 (2017).
57. J. Warneke, M. Rohdenburg, Y. Zhang, J. Orszagh, A. Vaz, I. Utke, J.T.M. De Hosson, W.F. van Dorp, and P. Swiderek: Role of NH₃ in the electron-induced reactions of adsorbed and solid cisplatin. *J. Phys. Chem. C* **120**, 4112 (2016).
58. J. Kopyra, C. Koenig-Lehmann, I. Bald, and E. Illenberger: A single slow electron triggers the loss of both chlorine atoms from the anticancer drug cisplatin: implications for chemoradiation therapy. *Angew. Chem. Int. Ed.* **48**, 7904 (2009).
59. S.N. Pham, J.E. Kuether, M.J. Gallagher, R.T. Hernandez, D.N. Williams, B. Zhi, A.C. Mensch, R.J. Hamers, Z. Rosenzweig, H. Fairbrother, M.O. P. Krause, Z.V. Feng, and C.L. Haynes: Carbon dots: a modular activity to teach fluorescence and nanotechnology at multiple levels. *J. Chem. Ed.* **94**, 1143 (2017).
60. G.V. Naik, V.M. Shalaev, and A. Boltasseva: Alternative Plasmonic Materials: Beyond Gold and Silver. *Adv. Mater.* **25**, 3264 (2013).
61. T.H. Baum: Laser chemical vapor deposition of gold: the effect of organometallic structure. *J. Electrochem. Soc.* **134**, 2616 (1987).
62. H.W.P. Koops, J. Kretz, M. Rudolph, M. Weber, G. Dahm, and K.L. Lee: Characterization and application of materials grown by electron-beam-induced deposition. *Jpn. J. Appl. Phys.* **33**, 7099 (1994).
63. I. Utke, M.G. Jenke, C. Roling, P.H. Thiesen, V. Iakovlev, A. Sirbu, A. Meruta, A. Caliman, and E. Kapon: Polarisation stabilisation of vertical cavity surface emitting lasers by minimally invasive focused electron beam triggered chemistry. *Nanoscale*. **3**, 2718 (2011).
64. M.G. Jenke, D. Lerosé, C. Niederberger, J. Michler, S. Christiansen, and I. Utke: Toward local growth of individual nanowires on three-dimensional microstructures by using a minimally invasive catalyst templating method. *Nano Lett.* **11**, 4213 (2011).
65. A. Folch, J. Servat, J. Esteve, J. Tejada, and M. Seco: High-vacuum versus "environmental" electron beam deposition. *J. Vac. Sci. Technol. B* **14**, 2609 (1996).
66. T. Brintlinger, M.S. Fuhrer, J. Melngailis, I. Utke, T. Bret, A. Perentes, P. Hoffmann, M. Abourida, and P. Doppelt: Electrodes for carbon nanotube devices by focused electron beam induced deposition of gold. *J. Vac. Sci. Technol. B* **23**, 3174 (2005).
67. P. Hoffmann, I. Utke, F. Cicoira, B. Dwir, K. Leifer, E. Kapon, and P. Doppelt: Focused electron beam induced deposition of gold and rhodium. *Mater. Res. Soc. Symp. Proc.* **624**, 171 (2001).
68. I. Utke, P. Hoffmann, B. Dwir, K. Leifer, E. Kapon, and P. Doppelt: Focused electron beam induced deposition of gold. *J. Vac. Sci. Technol. B* **18**, 3168 (2000).
69. I. Utke, B. Dwir, K. Leifer, F. Cicoira, P. Doppelt, P. Hoffmann, and E. Kapon: Electron beam induced deposition of metallic tips and wires for microelectronics applications. *Microelectron. Eng.* **53**, 261 (2000).
70. W. Fuß and M. Rühle: Chlor(trifluorophosphan)gold(I), eine einfache flüchtige Goldverbindung. *Z. Naturforsch. B* **47**, 591 (1992).
71. J.J.L. Mulders, J.M. Veerhoek, E.G.T. Bosch, and P.H.F. Trompenaars: Fabrication of pure gold nanostructures by electron beam induced deposition with Au(CO)Cl precursor: deposition characteristics and primary beam scattering effects. *J. Phys. D Appl. Phys.* **45**, 475301 (2012).
72. P.G. Jones: The crystal structure of carbonyl gold(I) chloride, (OC)AuCl. *Z. Naturforsch. B* **37**, 823 (1982).
73. D. Belli Dell'Amico and F. Calderazzo: Convenient methods for the preparation of anhydrous gold(III) chloride and chlorocarbonylgold(I). *Gazz. Chim. Ital.* **103**, 1099 (1973).
74. P.D. Tran and P. Doppelt: Gold CVD using trifluorophosphine gold(I) chloride precursor and its toluene solutions. *J. Electrochem. Soc.* **154**, D520 (2007).
75. M.S. Kharasch and H.S. Isbell: Chemistry of organic gold compounds. I. Aurous chloride carbonyl and a method of linking carbon to carbon. *J. Am. Chem. Soc.* **52**, 2919 (1930).
76. W. van Dorp, X. Wu, J. Mulders, S. Harder, P. Rudolf, and J. De Hosson: Gold complexes for focused-electron-beam-induced deposition. *Langmuir* **30**, 12097 (2014).
77. W.G. Carden, J. Pedziwiatr, K.A. Abboud, and L. McElwee-White: Halide effects on the sublimation temperature of X–Au–L complexes: implications for their use as precursors in vapor phase deposition methods. *ACS Appl. Mater. Interfaces* **9**, 40998 (2017).
78. D.S. Eggleston, D.F. Chodosh, R.L. Webb, and L.L. Davis: (Tert-butyl isocyanide)chlorogold(I). *Acta Crystallogr. C* **42**, 36 (1986).
79. W. Schneider, K. Angermaier, A. Sladek, and H. Schmidbauer: Ligand influences on the supramolecular chemistry of simple gold(I) complexes. Mononuclear (isonitrile)gold(I) complexes. *Z. Naturforsch. B Chem. Sci.* **51**, 790 (1996).
80. R.-Y. Liao, T. Mathieson, A. Schier, R.J.F. Berger, N. Runeberg, and H. Schmidbauer: Structural, spectroscopic and theoretical studies of (t-butyl-isocyanide)gold(I) iodide. *Z. Naturforsch. B Chem. Sci.* **57**, 881 (2002).
81. O. Elbjairami, M.W.A. Gonser, B.N. Stewart, A.E. Bruce, M.R.M. Bruce, T.R. Cundari, and M.A. Omary: Luminescence, structural, and bonding trends upon varying the halogen in isostructural aurophilic dimers. *Dalton Trans.*, 1522 (2009).
82. K. Angermaier, E. Zeller, and H. Schmidbauer: Crystal-structures of chloro(trimethylphosphine)gold(I), chloro(tri-n-propylphosphine)gold(I) and bis(trimethylphosphine)gold(I) chloride. *J. Organomet. Chem.* **472**, 371 (1994).
83. K. Angermair, G.A. Bowmaker, E.N. de Silva, P.C. Healy, B.E. Jones, and H. Schmidbauer: Vibrational and solid-state phosphorus-31 nuclear magnetic resonance spectroscopic studies of 1:1 complexes of PPh₃ with gold(I) halides; crystal structure of [AuBr(PMe₃)]. *J. Chem. Soc. Dalton Trans.*, 3121 (1996).
84. A. Ahrland, K. Dreisch, B. Noren, and A. Oskarsson: Crystal structures of Iod(triphenylphosphine)gold(I) and bis(Iodo(trimethylphosphine)gold(I)). *Acta Chem. Scand.* **41A**, 173 (1987).
85. A. Bauer, N.W. Mitzel, A. Schier, D.W.H. Rankin, and H. Schmidbauer: Tris(dimethylamino)phosphane as a new ligand in gold(I) chemistry: synthesis and crystal structures of (Me₂N)₃PAuCl, {¹(Me₂N)₃PAu₃O}+BF₄⁻, {¹(Me₂N)₃PAu₃NP(NMe₂)₃}²⁺{BF₄}⁻² and the precursor molecule (Me₂N)₃PNSiMe₃. *Chem. Ber.* **130**, 323 (1997).
86. A. Marashdeh, T. Tiesma, N.J.C. van Velzen, S. Harder, R.W.A. Havenith, J.T.M. De Hosson, and W.F. van Dorp: The rational design of a Au(I) precursor for focused electron beam induced deposition. *Beilstein J. Nanotechnol.* **8**, 2753 (2017).
87. F. Porrati, E. Begun, M. Winhold, H.S. Ch, R. Sachser, A.S. Frangakis, and M. Huth: Room temperature L1 0 phase transformation in binary CoPt nanostructures prepared by focused-electron-beam-induced deposition. *Nanotechnology* **23**, 185702 (2012).
88. R.C. Che, M. Takeguchi, M. Shimojo, W. Zhang, and K. Furuya: Fabrication and electron holography characterization of FePt alloy nanorods. *Appl. Phys. Lett.* **87**, 223109 (2005).
89. M.M. Shawrav, D. Belic, M. Gavagnin, S. Wachter, M. Schinnerl, H. D. Wanzenboeck, and E. Bertagnolli: Electron beam-induced CVD of nanoalloys for nanoelectronics. *Chem. Vap. Deposition* **20**, 251 (2014).
90. M. Winhold, C.H. Schwab, F. Porrati, R. Sachser, A.S. Frangakis, B. Kämpken, A. Terfort, N. Auner, and M. Huth: Binary Pt–Si nanostructures prepared by focused electron-beam-induced deposition. *ACS Nano* **5**, 9675 (2011).
91. F. Porrati, B. Kämpken, A. Terfort, and M. Huth: Fabrication and electrical transport properties of binary Co–Si nanostructures prepared by focused electron beam-induced deposition. *J. Appl. Phys.* **113**, 053707 (2013).
92. L. Bernau, M. Gabureac, R. Erni, and I. Utke: Tunable nanosynthesis of composite materials by electron-impact reaction. *Angew. Chem. Int. Ed.* **49**, 8880 (2010).
93. Z. Zhao, A. Fisher, Y. Shen, and D. Cheng: Magnetic properties of Pt-based nanoalloys: a critical review. *J. Cluster Sci.* **27**, 817 (2016).

94. J.M. Gaskell, A.C. Jones, H.C. Aspinall, S. Przybylak, P.R. Chalker, K. Black, H.O. Davies, P. Taechakumpot, S. Taylor, and G. W. Critchlow: Liquid injection ALD and MOCVD of lanthanum aluminate using a bimetallic alkoxide precursor. *J. Mater. Chem.* **16**, 3854 (2006).
95. M.J. Crosbie, P.J. Wright, H.O. Davies, A.C. Jones, T.J. Leedham, P. O'Brien, and G.W. Critchlow: MOCVD of strontium tantalate thin films using novel bimetallic alkoxide precursors. *Chem. Vap. Deposition* **5**, 9 (1999).
96. S. Abu Bakar, S. Tajammul Hussain, and M. Mazhar: CdTiO₃ thin films from an octa-nuclear bimetallic single source precursor by aerosol assisted chemical vapor deposition (AACVD). *New J. Chem.* **36**, 1844 (2012).
97. S.-G. Shyu, J.-S. Wu, S.-H. Chuang, K.-M. Chi, and Y.-S. Sung: Mixed-metal oxide films via a heterobimetallic complex as an MOCVD single-source precursor. *Chem. Commun.*, 2239 (1996).
98. E.P. Boyd, D.R. Ketchum, H. Deng, and S.G. Shore: Chemical vapor deposition of metallic thin films using homonuclear and heteronuclear metal carbonyls. *Chem. Mater.* **9**, 1154 (1997).
99. C.L. Czekaj and G.L. Geoffroy: Chemical vapor deposition of iron-cobalt (FeCo_x) and iron cobalt oxide (FeCo_xO_y) thin films from iron cobalt carbonyl clusters. *Inorg. Chem.* **27**, 8 (1988).
100. F. Porra, M. Pohlitz, J. Müller, S. Barth, F. Biegger, C. Gspan, H. Plank, and M. Huth: Direct writing of CoFe alloy nanostructures by focused electron beam induced deposition from a heteronuclear precursor. *Nanotechnology* **26**, 475701 (2015).
101. R. Kumar T.P., P. Weirich, L. Hrachowina, M. Hanefeld, R. Bjornsson, H. R. Hrodmarsson, S. Barth, D.H. Fairbrother, M. Huth, and O. Ingólfsson: Electron interactions with the heteronuclear carbonyl precursor H₂FeRu₃(CO)₁₃ and comparison with HFeCo₃(CO)₁₂: from fundamental gas phase and surface science studies to focused electron beam induced deposition. *Beilstein J. Nanotechnol.* **9**, 555 (2018).
102. C.J. Gilmore and P. Woodward: Crystal and molecular structure of H₂FeRu₃(CO)₁₃; a tetrahedral hydridocarbonyl of iron and ruthenium containing asymmetric carbon bridges. *J. Chem. Soc. A*, 3453 (1971).
103. L.-Y. Hsu, A.A. Bhattacharyya, and S.G. Shore: Structure of a second form of 1,2;2,3-di-μ-hydrido-μ₃-tetracarbonylferrio-cyclo-tris(tricarbonylruthenium)(3Ru-Ru), H₂FeRu₃(CO)₁₃. *Acta Crystallogr. C* **40**, 722 (1984).
104. T.P. Ragesh Kumar, I. Unlu, S. Barth, O. Ingólfsson, and D. H. Fairbrother: Electron induced surface reactions of HFeCo₃(CO)₁₂, a bimetallic precursor for focused electron beam induced deposition (FEBID). *J. Phys. Chem. C* **122**, 2648 (2018).
105. I. Unlu, J.A. Spencer, K.R. Johnson, R. Thorman, O. Ingólfsson, L. McElwee-White, and D.H. Fairbrother: Electron induced surface reactions of (η⁵-C₅H₅)Fe(CO)₂Mn(CO)₅, a potential heterobimetallic precursor for focused electron beam induced deposition (FEBID). *Phys. Chem. Chem. Phys.* **20**, 7862 (2018).
106. R.M. Thorman, I. Unlu, K.R. Johnson, R. Bjornsson, L. McElwee-White, H. Fairbrother, and O. Ingólfsson: Low energy electron-induced decomposition of (η⁵-Cp)Fe(CO)₂Mn(CO)₅, a potential bimetallic precursor for focused electron beam induced deposition of alloy structures. *Phys. Chem. Chem. Phys.* **20**, 5644 (2018).
107. Y.S. Won, Y.S. Kim, T.J. Anderson, and L. McElwee-White: Computational study of the gas phase reactions of isopropylimido and allylimido tungsten precursors for chemical vapor deposition of tungsten carbonitride films: implications for the choice of carrier gas. *Chem. Mater.* **20**, 7246 (2008).
108. Y.S. Won, Y.S. Kim, T.J. Anderson, L.L. Reifort, I. Ghiviriga, and L. McElwee-White: Homogeneous decomposition of aryl- and alkylimido precursors for the CVD of tungsten nitride: a combined density functional theory and experimental study. *J. Am. Chem. Soc.* **128**, 13781 (2006).
109. S. Engmann, M. Stano, P. Papp, M.J. Brunger, S. Matejcek, and O. Ingólfsson: Absolute cross sections for dissociative electron attachment and dissociative ionization of cobalt tricarbonyl nitrosyl in the energy range from 0 eV to 140 eV. *J. Chem. Phys.* **138**, 044305/1 (2013).
110. C.R. Arumainayagam, H.-L. Lee, R.B. Nelson, D.R. Haines, and R. P. Gunawardane: Low-energy electron-induced reactions in condensed matter. *Surf. Sci. Rep.* **65**, 1 (2010).